Report

Current Biology

# Processive Kinesin-14 HSET Exhibits Directional Flexibility Depending on Motor Traffic

## Highlights

- Loaded HSET takes processive steps at the single-molecule level
- HSET's tail interaction with E-hooks enables long range unloaded transport
- HSET brakes against Eg5 force generation in anti-parallel bundles via motor heads
- HSET's collective bidirectionality is compliant to Eg5 in anti-parallel bundles

## Authors

Dana N. Reinemann, Stephen R. Norris, Ryoma Ohi, Matthew J. Lang

## Correspondence

matt.lang@vanderbilt.edu

## In Brief

Reinemann et al. investigate kinesin-14 HSET force generation at the single-molecule level and in microtubule bundles using optical tweezers. HSET contains both diffusive and processive single molecule properties that collectively move bidirectionally and antagonize Eg5 force generation in anti-parallel bundles.

Reinemann et al., 2018, Current Biology *28*, 2356–2362
July 23, 2018 
https://doi.org/10.1016/j.cub.2018.06.055

CellPress

CellPress

Current Biology
Report

# Processive Kinesin-14 HSET Exhibits Directional Flexibility Depending on Motor Traffic

Dana N. Reinemann,[1] Stephen R. Norris,[2] Ryoma Ohi,[3] and Matthew J. Lang[1,4,5,*]
[1]Department of Chemical and Biomolecular Engineering, Vanderbilt University, Nashville, TN 37235, USA
[2]Department of Cell and Developmental Biology, Vanderbilt University, Nashville, TN 37232, USA
[3]Department of Cell and Developmental Biology and LSI, University of Michigan School of Medicine, Ann Arbor, MI 48109-2216, USA
[4]Department of Molecular Physiology and Biophysics, Vanderbilt University Medical Center, Nashville, TN 37232, USA
[5]Lead Contact
*Correspondence: matt.lang@vanderbilt.edu
https://doi.org/10.1016/j.cub.2018.06.055

## SUMMARY

**A common mitotic defect observed in cancer cells that possess supernumerary (more than two) centrosomes is multipolar spindle formation [1, 2]. Such structures are resolved into a bipolar geometry by minus-end-directed motor proteins, such as cytoplasmic dynein and the kinesin-14 HSET [3–8]. HSET is also thought to antagonize plus-end-directed kinesin-5 Eg5 to balance spindle forces [4, 5, 7, 9]. However, the biomechanics of this force opposition are unclear, as HSET has previously been defined as a non-processive motor [10–16]. Here, we use optical trapping to elucidate the mechanism of force generation by HSET. We show that a single HSET motor has a processive nature with the ability to complete multiple steps while trapped along a microtubule and when unloaded can move in both directions for microns. Compared to other kinesins, HSET has a relatively weak stall force of 1.1 pN [17, 18]. Moreover, HSET's tail domain and its interaction with the E-hook of tubulin are necessary for long-range motility. *In vitro* polarity-marked bundle assays revealed that HSET selectively generates force in anti-parallel bundles on the order of its stall force. When combined with varied ratios of Eg5, HSET adopts Eg5's directionality while acting as an antagonizing force brake, requiring at least a 10-fold higher Eg5 concentration to surpass HSET's sliding force. These results reveal HSET's ability to change roles within the spindle from acting as an adjustable microtubule slider and force regulator to a processive motor that aids in minus end focusing.**

## RESULTS

### FL-HSET Generates Weak Force at the Single-Molecule Level

FL-HSET was investigated at the single-molecule level using optical tweezers to determine the force generation and processive capabilities of the motor in a loaded environment (Figure 1A). FL-HSET was able to generate force with structured stepping and a defined stall, or maximum force (Figure 1B). HSET runs do not have a traditional plateaued stall like kinesin-1, falling off abruptly after reaching a maximum force, as seen with other motors [18–20]. Step sizes and dwell times were measured for forward and backward steps (Figures 1C and 1D). FL-HSET takes 8 nm steps, corresponding to the lattice spacing of tubulin dimers, with a smaller population of 16 nm steps. FL-HSET can also take backward steps ~33% of the time. The average stall force of FL-HSET (Figure 1E) was very weak (1.1 pN) in comparison to that of kinesin-1 [17, 21].

The force-velocity relationship exhibited by FL-HSET (Figure 1F) was fit to a one-parameter force-velocity equation (Table S1) [22], and the Boltzmann relation models the data well. The fitting also reveals that HSET is biochemically limited, which is consistent with previous kinetic analysis of Ncd [12]. The characteristic transition state distance of 10.4 nm is close to the measured step size of HSET and 9 nm working strokes from the three-bead optical trap assay [11]. As demonstrated in Figure 2, FL-HSET at the single-molecule level has a diffusive nature.

### Unloaded FL-HSET Moves Microns along Microtubules

The behavior of FL-HSET without the confines of the trap was investigated to evaluate the role of load in motor motility. Unloaded FL-HSET at the single-molecule level attached to a bead was evaluated using a video-tracking algorithm (STAR Methods). A representative trace of unloaded HSET is in Figure 2A. Strikingly, persistent travel over microns long distances is observed in both directions over a time span of minutes. Mean squared displacement (MSD) analysis was performed to parameterize whether the observed motion was directed or diffusive like (Figure 2B). In averaging the points over the first 20 s of each trace, the MSD was linear, with a calculated diffusion constant of $5.9 \times 10^4$ nm$^2$/s. Figure 2C shows how dwell finding analysis was used to parameterize how far HSET moved before changing directions (STAR Methods).

Directional persistence of HSET was evaluated by measuring the distance traveled before switching directions (Figure 2D). From this analysis, FL-HSET has no directional bias as an unloaded single molecule (see Figure 2A). The time spent traveling in either direction was evaluated similarly (Figure 2E). There is a substantial difference between the long-distance, unloaded diffusive-like motion and directed motility related to loaded

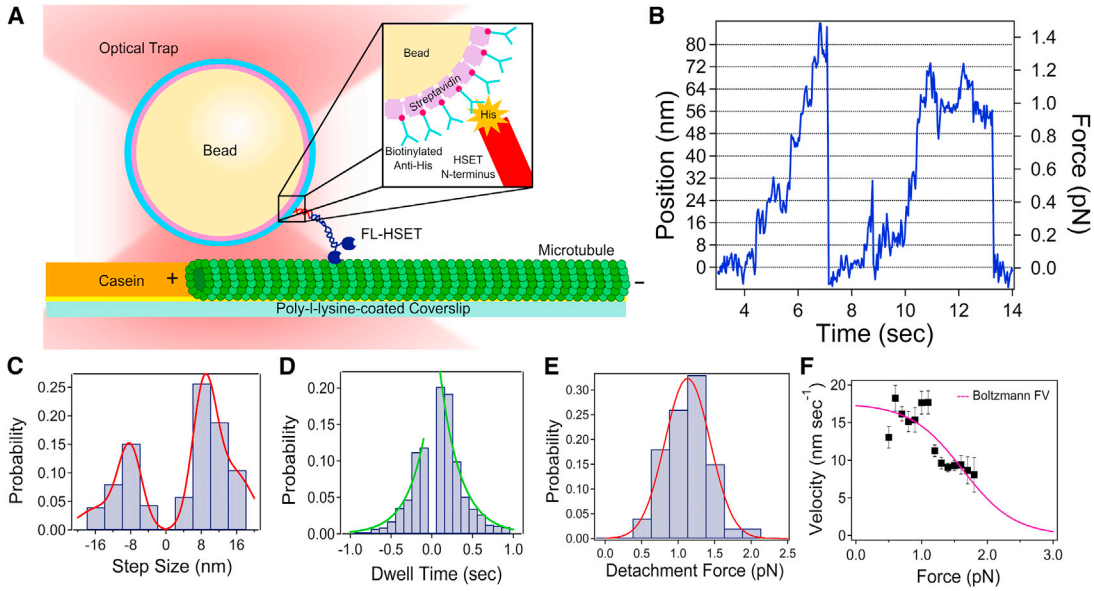


**Figure 1. FL-HSET Is Weakly Processive Under Load**

(A) Schematic of the loaded motility assay.

(B) Representative trace of a single FL-HSET (full-length) motor walking along a microtubule, taking consecutive steps, reaching a stall force, and then returning to the trap center.

(C) The forward (minus-end-directed) step size of HSET distribution fit to a double Gaussian is 8.7 ± 2.7 nm and 15.6 ± 4.2 nm (average ± SD; n = 918). The backward (plus-end-directed) step size, also fit to a double Gaussian, is 8.2 ± 2.7 nm and 15.4 ± 4.4 nm (n = 465). The 16 nm steps could be due to the diffusive element of the motor taking over briefly or two very fast 8 nm steps in succession that could not be resolved by our step/dwell-finding algorithm.

(D) Exponential fits for dwell times between steps yield a forward time constant of $k^{-1}$ = 0.25 s and backward time constant of $k^{-1}$ = 0.23 s.

(E) The average detachment force, or apparent stall force, of HSET is 1.1 ± 0.34 pN (n = 100).

(F) Force-velocity data (error bars indicate the SEM) were fit to the Boltzmann kinetic model.

See also Table S1.

force-velocity measurements, suggesting that loaded and unloaded HSET behave quite differently. Interestingly, calculation of an MSD from simulated 1D random walks reveals trajectories that are consistent with experiments, further showing that diffusion dominates unloaded transport (Figure S1).

The unloaded assay was repeated on subtilisin-digested microtubules, in which the E-hook, or negatively charged C-terminal tail, is cleaved [19, 23]. Under single-molecule conditions with unaltered microtubules, 11% of beads (n = 65 beads) showed binding and apparent diffusive-like movement, as shown in Figure 2. When the assay was repeated with digested microtubules, beads would not bind microtubules (n = 60 beads). These results reveal that the E-hook, most likely through electrostatic interactions, is necessary for initial binding and subsequent persistent HSET motility due to transient binding of the tail to adjacent E-hooks.

## HSET Tail Domain Is Required for Substantial Transport

A tailless HSET construct (HSET-ΔT) was made to evaluate the role of the N-terminal tail domain in microtubule targeting, force generation, and processivity. Ncd's tail has been shown to be critical for microtubule-microtubule crosslinking and sliding [6, 8, 24]. We carried out unloaded experiments using HSET-ΔT (Figure S2). The results revealed a drastic decrease in velocity and overall motility (only moving 40% of the time) and switching to unidirectional motion (Figure 2A, inset). In conjunction with FL-HSET on digested microtubules, these results suggest that the tail domain is necessary for consistent binding to microtubules and larger amplitude diffusive-like transport, as well as that the E-hook most likely plays an important role in maintaining HSET-microtubule association.

To determine whether the tail facilitates transient association or strong, tension-building binding to microtubules, we investigate HSET-ΔM (no motor) in rupture assays to observe bond lifetime at a defined force (Figure 3A; STAR Methods) [19]. Beads were trapped and positioned over a microtubule to facilitate attachment. Tethers were quickly pulled to a pre-defined force range and held until rupture. Lifetime and rupture force experiments on normal microtubules were fit to bimodal distributions (Figures 3B and 3C). Although the bond is short lived, the tail quickly rebinds the microtubule, allowing for multiple measurements, and reflects unloaded HSET's extended association with the microtubule, most likely through binding adjacent E-hooks.

Binding experiments were repeated on digested microtubules (Figure 3D) [23]. The lifetime and force at rupture measurements shifted favoring a single distribution (Figures 3E and 3F). We note that the observed probability distributions depend on the force range sampled, high or low force distributions; however, for our sampled forces, a general shift to lower lifetimes on digested microtubules (Figure 3G) is seen. The lifetime-force relationship was fit to the Bell model, which describes force dependent binding for biological interactions (Figure 3G) [25]. The distance to the transition state, which refers to the mechanical compliance of

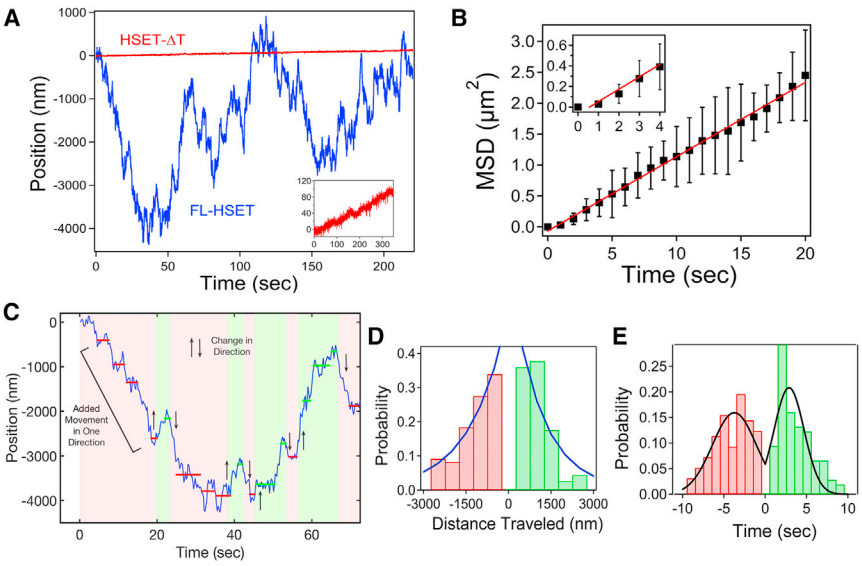


**Figure 2. HSET Moves Bidirectionally in an Unloaded Assay**

(A) Representative trace of a single HSET (full-length) moving along a microtubule. The trace shows bidirectional movement and association with the microtubule for minutes at a time. The inset shows a comparison to HSET-ΔT motility (Figure S2).

(B) MSD analysis reveals a diffusion constant $D = 5.9 \times 10^4$ nm$^2$/s. The inset shows the initial deviation from linearity.

(C) The step/dwell-finding algorithm (STAR Methods) demonstrated with the first 70 s of the trace in (A). Red dwells indicate movement toward one end, and green dwells toward the other. Successive movements in one direction were added together to determine how far HSET moved before changing directions.

(D) Distributions showing the distance traveled in each direction before changing directions. HSET moves $k^{-1}$ = 1,080 nm (n = 113) in one direction and $k^{-1}$ = 1,310 nm (n = 117) in the other before changing directions, showing no preference for movement in either direction.

(E) Distributions showing the time traveled in each direction. HSET moves 3.7 ± 2.6 s toward one end and 2.9 ± 1.8 s toward the other before changing directions.

See also Figures S1 and S2.

the motor, was calculated from each fit with values for HSET-ΔM of 0.52 nm (microtubules) and 0.92 nm (digested). Together, these results reveal that the tail interacts most strongly with the E-hook but also has some association with the microtubule lattice. Interestingly, the lattice interaction lifetime of 0.22 s is similar to the average dwell time between steps.

## HSET Acts as a Force Brake against Eg5

Although the interplay of Eg5 and HSET has been investigated previously in cells [4, 7], regulation of force generation in microtubule bundles has not been explored *in vitro*. To elucidate the role HSET plays with Eg5 in the spindle, an *in vitro* microtubule bundle assay with known microtubule orientation was utilized at different Eg5:HSET ratios (Figure 4A). Force-generating capabilities of HSET alone in bundles were investigated using ~20 nM HSET (Figure 4B). As shown previously [6, 8], parallel bundles become locked (red) with an antagonizing baseline signature. In anti-parallel bundles (blue), HSET generates a slow force ramp that plateaus at 2.2 pN. As discussed below, anti-parallel bundles formed with HSET alone can transport the cargo microtubule in both directions, suggesting that HSET can serve as a flexible microtubule crosslinker.

Subsequently, different ratios of Eg5 were added to HSET bundles to evaluate HSET's effect on Eg5 force generation in bundles formed before trapping measurements took place (Figure 4C). We characterized Eg5 bundle motility alone (~20 nM) and determined that under these conditions, the average plateau force for Eg5 was significantly higher at 6.8 pN. Next, the following Eg5:HSET molar solution ratios were employed through titrating Eg5: 10:1 (orange), 2:1 (yellow), 1:1 (green), and 1:2 (blue). HSET or Eg5 alone is shown in purple or red, respectively. We note that solution ratios may differ somewhat from ratios in bundle overlaps, and overlap lengths were not directly measured. Even so, although Eg5 at the single-molecule level is stronger (stall force of dimer ~5 pN [17], tetramer ~2 pN [18]) than HSET (stall force ~1 pN), HSET appears to control the bundle force and velocity characteristics (see Table S2). Plateau forces remain around that of HSET alone in the combined assays. The plateau force increased from an average between 2 and 3 pN to almost 5 pN for 10:1 Eg5:HSET. Repeating the 1:1 ratio with Eg5:HSET-ΔT revealed a similar plateau force to 1:1 Eg5:FL-HSET, indicating that force and velocity braking is most likely dominated by the motor heads through a potential traffic jam mechanism (Table S2) or somehow altering Eg5 properties through the microtubule lattice (see Discussion) [26, 27]. Additionally, HSET-ΔT cannot form bundles, revealing that the tail domain is essential for bundle formation (Table S2) with HSET alone. Although similar braking via the motor heads was seen with and without the tail, the motors with tail domains can still crosslink microtubules and jam motor traffic. We note HSET may contain a second weak microtubule binding domain that does not appear sufficient to form bundles but, once formed, may contribute to the observed braking [28].

To evaluate whether HSET's flexible motility has an effect when in combination with Eg5 in bundles, we evaluated the direction of bundle microtubule movement (Figure 4D). Bundle orientation was noted by polarity markings (STAR Methods), and the relative direction of cargo microtubule/bead movement was recorded. In anti-parallel bundles with HSET alone, the bead was persistently pushed and/or pulled out of the trap, indicating that teams of HSET motors can possibly move together in both directions in bundles. Here, "push" refers to the cargo microtubule moving the bead from the trap center and farther away from the substrate microtubule, and "pull" refers to the cargo microtubule moving the bead closer toward the substrate microtubule. In anti-parallel bundles with Eg5

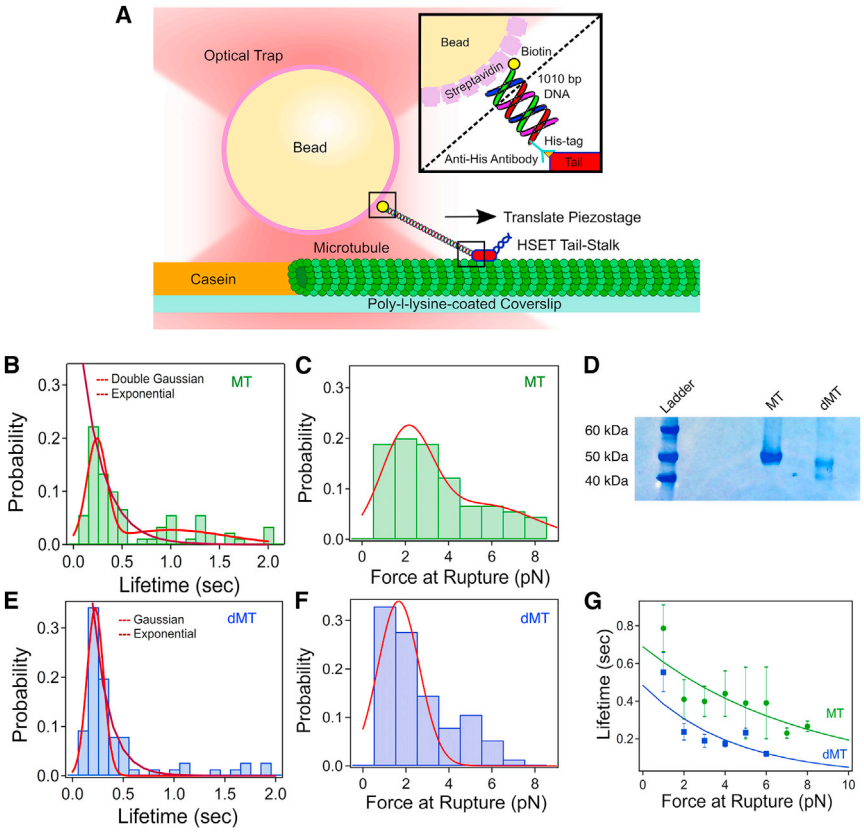


**Figure 3. HSET Tail Domain Interacts with E-Hooks**

(A) Assay schematic.

(B) Lifetime distribution for Tail-Stalk (HSET-ΔM) on normal microtubules. There was a double Gaussian distribution, with averages of 0.29 ± 0.07 s (average ± SD) and 1.0 ± 0.6 s (n = 90). Single exponential fits yield a time constant of $k^{-1}$ = 0.23 s.

(C) The force at rupture for Tail-Stalk on normal microtubules was 2.1 ± 1.2 pN and 5.6 ± 2.3 pN.

(D) SDS-PAGE gel confirming successful E-hook digestion.

(E) The double Gaussian lifetime distribution collapsed down to a single for digested microtubules, 0.22 ± 0.08 s (n = 76), and a time constant of $k^{-1}$ = 0.16 s.

(F) The force at rupture for digested microtubules was 2.0 ± 0.7 pN.

(G) The force-lifetime relationship follows the Bell model showing distinct binding modes on the two microtubule types. The extracted distances to the transition state are 0.52 nm on microtubule and 0.92 nm on digested microtubules.

alone, the bead was solely pushed through the trap. Since the bead is on the minus end of the cargo microtubule and Eg5 is plus-end directed, the cargo microtubule can only be pushed through the trap. Interestingly, in all cases where both HSET and Eg5 are in anti-parallel bundles, the bead is solely pushed through the trap, suggesting that Eg5 motility dictates HSET directionality within bundle overlaps. HSET's directional flexibility thus allows it to be compliant in bundles when a stronger motor is present. However, Eg5 does not overtake HSET in generating force. As shown in Table S2, HSET's presence significantly decreases force generation in combined motor bundles. Together, these data show that HSET acts as a force brake against Eg5, but is also compliant, allowing others to dictate direction, permitting sensitive and complex force regulation in anti-parallel overlaps.

## DISCUSSION

As single molecules, kinesin-14s of the animal kingdom (ncd, XCTK2, and HSET) do not exhibit properties that readily explain their capacity to self-assemble microtubule asters [5, 29], regulate force balance within a bipolar spindle, or coalesce supernumerary centrosomes into two spindle poles [30]. Single molecules of metazoan kinesin-14s are typically regarded to be non-processive motors [8, 10, 12, 14, 16, 28, 31, 32] that generate negligible levels of force [14]. Our results are generally consistent with these previous findings, but we did observe human HSET to take multiple 8 nm steps and stall at 1.1 pN. These features would allow HSET to productively build up force on the scale of ~100 nm. Also consistent with previous work [33], we observed single unloaded HSET molecules to diffuse over microns-long distances. This diffusive motion is facilitated by the tail domain's interaction with the E-hook and may enable HSET to efficiently target critical architectures that it acts to remodel (such as bundles and asters) in addition to promoting its ability to generate entropic forces [33, 34].

Closer examination of HSET's diffusive motion reveals key points. The experimental diffusion constant ($D = 5.9 \times 10^4$ nm$^2$/s) and the tail or motor domain lifetime ($t > 0.25$ s) suggest a step size $\delta = \sqrt{(2Dt)} > 171$ nm that is larger than the molecular size. Dwell times calculated from a ~50 nm molecular size result in 20 ms lifetimes, much shorter than those observed for tail and motor domain binding. Given the persistent association of HSET with the microtubule, it is likely that multiple binding modes and dwell time periods underpin the diffusive-like motion. Another explanation is that low loads and the presence of the tail domain "turns on" motility but in a bidirectional manner, as seen in bundles. Such motion can masquerade as diffusion.

HSET exhibited two novel activities in our two-microtubule assay: (1) alone, HSET promotes bidirectional sliding of anti-parallel microtubules, and (2) HSET determines the force magnitude that Eg5 generates in anti-parallel microtubule overlaps. The first result was unexpected, as HSET and Ncd have only been reported to drive unidirectional sliding [8, 33]. Our ability to detect bidirectional motion is most likely due to the sensitivity of our optical trap assay, in which small backward motions of microtubules can be resolved. How HSET drives bidirectional sliding is not clear, but it could be caused by its propensity to take backward steps (~33%) or the result of an entropic force mechanism [33, 34]. Crosslinking microtubules with a motor element permits the generation of architectural elements with the strength of bundles while allowing for adjustments in length.

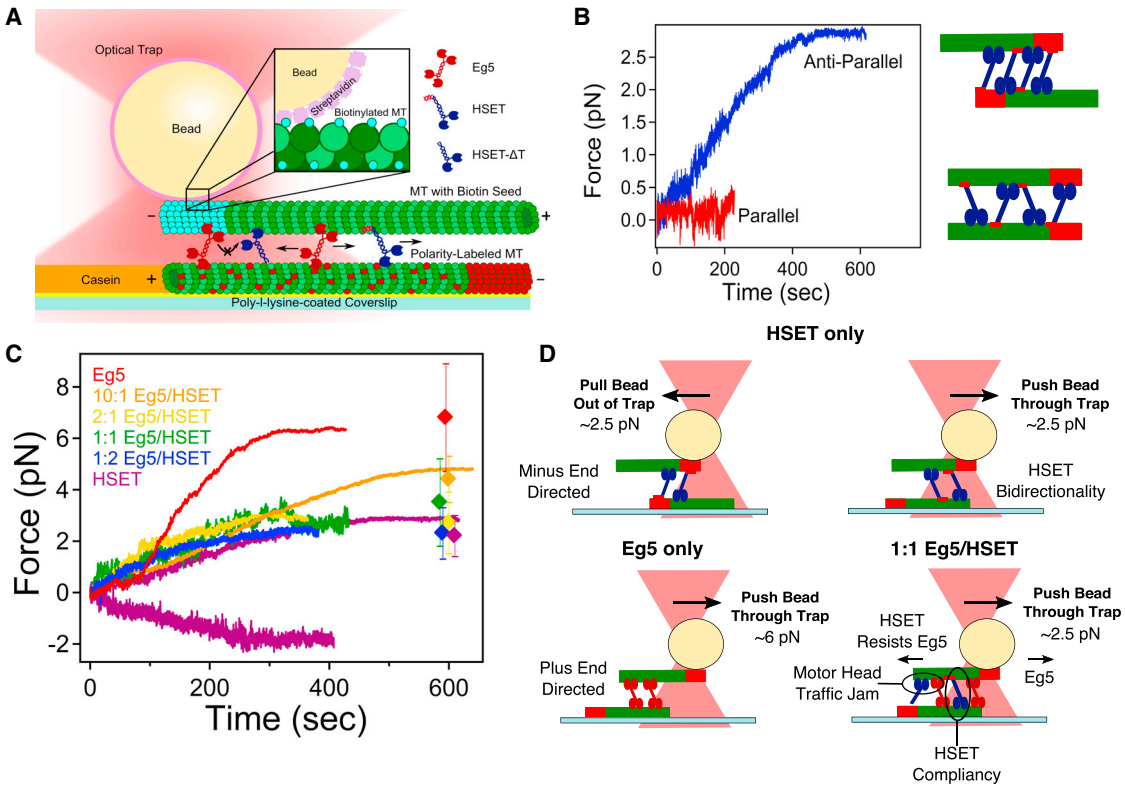


**Figure 4. HSET Acts as a Force Brake against Eg5 in Bundles**

(A) Bundle assay schematic.

(B) HSET selectively generates force in anti-parallel bundles (blue), whereas parallel bundles (red) become locked. In anti-parallel bundles (blue), HSET generates a slow force ramp that plateaus off at an average force of 2.2 ± 0.8 pN (average ± SD; n = 18).

(C) Representative traces of different motor molar ratios of Eg5 and HSET were utilized to determine how HSET at 20 nM affects titrated Eg5 force generation in bundles. Diamonds indicate average force plateau values.

(D) Direction of cargo microtubule movement in each bundle scenario. HSET is compliant to Eg5's direction of movement while still resisting Eg5's full force generation potential.

See also Figure S3 and Table S2.

When Eg5 and HSET are simultaneously present in microtubule overlaps, our studies reveal that it takes a significant proportion of Eg5 relative to HSET to overtake HSET force regulation. Furthermore, Eg5 dictates sliding direction, whereas HSET regulates force and velocity. This is reflective of previous simulation results in which Ncd facilitates motility through successive forming and breaking of multiple intermediate contacts between the motor head and neck domains [35], in contrast to a directed power stroke. Such guided, contact-dependent conformational change is supported by the long distance to transition state and large percentage of backsteps extracted in our single-molecule experiments. In contrast to a power stroke mechanism, turning on HSET may be more sensitive to subtleties relating to the local motor's orientation, local twisting, and proximity relative to the neighboring microtubule architecture. Our results suggest that direction can be controlled through neighboring motors. Here, Eg5 dominates the guided direction, but HSET determines the force magnitude. Strikingly, replacement of HSET with HSET-ΔT at a 1:1 ratio with Eg5 in bundles, along with the low force, short-lived interaction between the tail and microtubule, reveals that force and velocity braking is motor head associated and driven by potential mechanisms such as bundle traffic jams or potential disruption of the local microtubule lattice [26, 27]. Although tails interact weakly with microtubules and most likely do not contribute much to building up tension, their binding, and thus additional traffic backup, could also contribute to braking. Therefore, the major components that are likely to determine force regulation in bundles include opposition of Eg5 by HSET's motor heads, differing motor mechanics (power stroke versus guided diffusion) between Eg5 and HSET, and entropic contributions from overlap length and motor density.

Our work provides insight into why spindles lengthen upon kinesin-14 overexpression [4, 36], rather than collapsing as expected from high-levels from a minus-end-directed motor. Yeast Kar3 has been proposed to align anti-parallel microtubules at the spindle equator, thus providing a suitable substrate for Cin8 to drive pole separation [36]. Work by Braun et al. shows that HSET dissociates infrequently from microtubule overlap zones as a consequence of its two microtubule-binding domains [33], thus stabilizing an anti-parallel overlap zone. Another possibility is HSET's complex nature in bundles—being compliant with and resistive against Eg5. There may be a need to generate structures with the strength of bundled microtubules, but also permit sliding between microtubule elements to new overall lengths.

Other kinesins are also known to toggle between diffusive and motile states, such as Eg5, in which motility is activated upon motor head interactions with two anti-parallel tracks [9, 37]. Since HSET moves with Eg5's direction, this flexibility could explain spindle elongation as opposed to shortening upon overexpression. A final consideration is that the processivity of HSET can be dramatically increased upon its multimerization via soluble, unpolymerized tubulin (S.R.N. and R.O., unpublished data). This mode of regulation may toggle HSET's function between microtubule sliding and/or cross-linking to long-range microtubule transport, as occurs during aster formation or centrosome clustering.

In summary, the kinesin-14 HSET was demonstrated through single-molecule optical trapping to have a weakly processive nature. The tail domain is required for bidirectional movement and long-range motility through interacting with the E-hook. Thus, HSET can be diffusive like and processive simultaneously, and those qualities are important for HSET's function as a force regulator against Eg5 within the spindle. Future experiments that track the overlap lengths, numbers, and types of motors via fluorescence, and degrees of crosslinking present while monitoring force buildup and bundle dynamics will help define this subtle interplay [18]. Together, our results reflect HSET's ability to be physiologically relevant when centrosome number is not two, making it an attractive cancer therapy target.

## STAR★METHODS

Detailed methods are provided in the online version of this paper and include the following:

- KEY RESOURCES TABLE
- CONTACT FOR REAGENT AND RESOURCE SHARING
- EXPERIMENTAL MODEL AND SUBJECT DETAILS
- METHOD DETAILS
  - Molecular Biology and Baculovirus Construction
  - Protein Expression and Purification
  - Microtubule Preparation
  - Single Molecule Optical Trapping Assays
- QUANTIFICATION AND STATISTICAL ANALYSIS

### SUPPLEMENTAL INFORMATION

Supplemental Information includes three figures and two tables and can be found with this article online at https://doi.org/10.1016/j.cub.2018.06.055.

### ACKNOWLEDGMENTS

We are grateful for helpful discussions with William Hancock and Marija Zanic. This material is based upon work supported by the National Science Foundation Graduate Research Fellowship Program under grant no. 1445197 (D.N.R.). This work was also supported, in part, by the Singapore-MIT Alliance for Research and Technology–BioSym and NSF grant no. 1330792 (M.J.L). R.O. was supported by the NIH grant no. R01 GM086610 and is a scholar of the Leukemia and Lymphoma Society.

### AUTHOR CONTRIBUTIONS

D.N.R. was involved in all aspects of the work, including assay development, performing experiments, data analysis, and manuscript preparation. S.R.N. and R.O. expressed and purified the constructs. D.N.R., S.R.N., R.O., and M.J.L. designed the experiments. D.N.R., S.R.N., R.O., and M.J.L. prepared the manuscript.

### DECLARATION OF INTERESTS

The authors declare no competing financial interests.

Received: February 5, 2018
Revised: May 1, 2018
Accepted: June 21, 2018
Published: July 12, 2018

### REFERENCES

1. Kleylein-Sohn, J., Pöllinger, B., Ohmer, M., Hofmann, F., Nigg, E.A., Hemmings, B.A., and Wartmann, M. (2012). Acentrosomal spindle organization renders cancer cells dependent on the kinesin HSET. J. Cell Sci. *125*, 5391–5402.
2. Heald, R., and Khodjakov, A. (2015). Thirty years of search and capture: the complex simplicity of mitotic spindle assembly. J. Cell Biol. *211*, 1103–1111.
3. McDonald, H.B., Stewart, R.J., and Goldstein, L.S.B. (1990). The kinesin-like ncd protein of Drosophila is a minus end-directed microtubule motor. Cell *63*, 1159–1165.
4. Cai, S., Weaver, L.N., Ems-McClung, S.C., and Walczak, C.E. (2009). Kinesin-14 family proteins HSET/XCTK2 control spindle length by cross-linking and sliding microtubules. Mol. Biol. Cell *20*, 1348–1359.
5. Hentrich, C., and Surrey, T. (2010). Microtubule organization by the antagonistic mitotic motors kinesin-5 and kinesin-14. J. Cell Biol. *189*, 465–480.
6. Braun, M., Drummond, D.R., Cross, R.A., and McAinsh, A.D. (2009). The kinesin-14 Klp2 organizes microtubules into parallel bundles by an ATP-dependent sorting mechanism. Nat. Cell Biol. *11*, 724–730.
7. Mountain, V., Simerly, C., Howard, L., Ando, A., Schatten, G., and Compton, D.A. (1999). The kinesin-related protein, HSET, opposes the activity of Eg5 and cross-links microtubules in the mammalian mitotic spindle. J. Cell Biol. *147*, 351–366.
8. Fink, G., Hajdo, L., Skowronek, K.J., Reuther, C., Kasprzak, A.A., and Diez, S. (2009). The mitotic kinesin-14 Ncd drives directional microtubule-microtubule sliding. Nat. Cell Biol. *11*, 717–723.
9. Kapitein, L.C., Peterman, E.J.G., Kwok, B.H., Kim, J.H., Kapoor, T.M., and Schmidt, C.F. (2005). The bipolar mitotic kinesin Eg5 moves on both microtubules that it crosslinks. Nature *435*, 114–118.
10. deCastro, M.J., Ho, C.H., and Stewart, R.J. (1999). Motility of dimeric ncd on a metal-chelating surfactant: evidence that ncd is not processive. Biochemistry *38*, 5076–5081.
11. deCastro, M.J., Fondecave, R.M., Clarke, L.A., Schmidt, C.F., and Stewart, R.J. (2000). Working strokes by single molecules of the kinesin-related microtubule motor ncd. Nat. Cell Biol. *2*, 724–729.
12. Foster, K.A., and Gilbert, S.P. (2000). Kinetic studies of dimeric Ncd: evidence that Ncd is not processive. Biochemistry *39*, 1784–1791.
13. Butterfield, A.E., Stewart, R.J., Schmidt, C.F., and Skliar, M. (2010). Bidirectional power stroke by ncd kinesin. Biophys. J. *99*, 3905–3915.
14. Furuta, K., Furuta, A., Toyoshima, Y.Y., Amino, M., Oiwa, K., and Kojima, H. (2013). Measuring collective transport by defined numbers of processive and nonprocessive kinesin motors. Proc. Natl. Acad. Sci. USA *110*, 501–506.
15. Pechatnikova, E., and Taylor, E.W. (1999). Kinetics processivity and the direction of motion of Ncd. Biophys. J. *77*, 1003–1016.
16. Crevel, I.M., Lockhart, A., and Cross, R.A. (1997). Kinetic evidence for low chemical processivity in ncd and Eg5. J. Mol. Biol. *273*, 160–170.
17. Valentine, M.T., Fordyce, P.M., Krzysiak, T.C., Gilbert, S.P., and Block, S.M. (2006). Individual dimers of the mitotic kinesin motor Eg5 step processively and support substantial loads in vitro. Nat. Cell Biol. *8*, 470–476.
18. Shimamoto, Y., Forth, S., and Kapoor, T.M. (2015). Measuring pushing and braking forces generated by ensembles of kinesin-5 crosslinking two microtubules. Dev. Cell *34*, 669–681.

19. Reinemann, D.N., Sturgill, E.G., Das, D.K., Degen, M.S., Vörös, Z., Hwang, W., Ohi, R., and Lang, M.J. (2017). Collective Force Regulation in Anti-parallel Microtubule Gliding by Dimeric Kif15 Kinesin Motors. Curr. Biol. *27*, 2810–2820.e6.
20. Schroeder, H.W., 3rd, Hendricks, A.G., Ikeda, K., Shuman, H., Rodionov, V., Ikebe, M., Goldman, Y.E., and Holzbaur, E.L.F. (2012). Force-dependent detachment of kinesin-2 biases track switching at cytoskeletal filament intersections. Biophys. J. *103*, 48–58.
21. Svoboda, K., and Block, S.M. (1994). Force and velocity measured for single kinesin molecules. Cell *77*, 773–784.
22. Wang, M.D., Schnitzer, M.J., Yin, H., Landick, R., Gelles, J., and Block, S.M. (1998). Force and velocity measured for single molecules of RNA polymerase. Science *282*, 902–907.
23. Lakämper, S., and Meyhöfer, E. (2005). The E-hook of tubulin interacts with kinesin's head to increase processivity and speed. Biophys. J. *89*, 3223–3234.
24. Popchock, A.R., Tseng, K.F., Wang, P., Karplus, P.A., Xiang, X., and Qiu, W. (2017). The mitotic kinesin-14 KlpA contains a context-dependent directionality switch. Nat. Commun. *8*, 13999.
25. Bell, G.I. (1978). Models for the specific adhesion of cells to cells. Science *200*, 618–627.
26. Muto, E., Sakai, H., and Kaseda, K. (2005). Long-range cooperative binding of kinesin to a microtubule in the presence of ATP. J. Cell Biol. *168*, 691–696.
27. Krebs, A., Goldie, K.N., and Hoenger, A. (2004). Complex formation with kinesin motor domains affects the structure of microtubules. J. Mol. Biol. *335*, 139–153.
28. Furuta, K., and Toyoshima, Y.Y. (2008). Minus-end-directed motor Ncd exhibits processive movement that is enhanced by microtubule bundling in vitro. Curr. Biol. *18*, 152–157.
29. Surrey, T., Nedelec, F., Leibler, S., and Karsenti, E. (2001). Physical properties determining self-organization of motors and microtubules. Science *292*, 1167–1171.
30. Kwon, M., Godinho, S.A., Chandhok, N.S., Ganem, N.J., Azioune, A., Thery, M., and Pellman, D. (2008). Mechanisms to suppress multipolar divisions in cancer cells with extra centrosomes. Genes Dev. *22*, 2189–2203.
31. Case, R.B., Pierce, D.W., Hom-Booher, N., Hart, C.L., and Vale, R.D. (1997). The directional preference of kinesin motors is specified by an element outside of the motor catalytic domain. Cell *90*, 959–966.
32. Stewart, R.J., Semerjian, J., and Schmidt, C.F. (1998). Highly processive motility is not a general feature of the kinesins. Eur. Biophys. J. *27*, 353–360.
33. Braun, M., Lansky, Z., Szuba, A., Schwarz, F.W., Mitra, A., Gao, M., Lüdecke, A., Ten Wolde, P.R., and Diez, S. (2017). Changes in microtubule overlap length regulate kinesin-14-driven microtubule sliding. Nat. Chem. Biol. *13*, 1245–1252.
34. Lansky, Z., Braun, M., Lüdecke, A., Schlierf, M., ten Wolde, P.R., Janson, M.E., and Diez, S. (2015). Diffusible crosslinkers generate directed forces in microtubule networks. Cell *160*, 1159–1168.
35. Lakkaraju, S.K., and Hwang, W. (2011). Hysteresis-based mechanism for the directed motility of the Ncd motor. Biophys. J. *101*, 1105–1113.
36. Hepperla, A.J., Willey, P.T., Coombes, C.E., Schuster, B.M., Gerami-Nejad, M., McClellan, M., Mukherjee, S., Fox, J., Winey, M., Odde, D.J., et al. (2014). Minus-end-directed Kinesin-14 motors align antiparallel microtubules to control metaphase spindle length. Dev. Cell *31*, 61–72.
37. van den Wildenberg, S.M.J.L., Tao, L., Kapitein, L.C., Schmidt, C.F., Scholey, J.M., and Peterman, E.J.G. (2008). The homotetrameric kinesin-5 KLP61F preferentially crosslinks microtubules into antiparallel orientations. Curr. Biol. *18*, 1860–1864.
38. Sturgill, E.G., Norris, S.R., Guo, Y., and Ohi, R. (2016). Kinesin-5 inhibitor resistance is driven by kinesin-12. J. Cell Biol. *213*, 213–227.
39. Shin, Y., Du, Y., Collier, S.E., Ohi, M.D., Lang, M.J., and Ohi, R. (2015). Biased Brownian motion as a mechanism to facilitate nanometer-scale exploration of the microtubule plus end by a kinesin-8. Proc. Natl. Acad. Sci. USA *112*, E3826–E3835.
40. Gibson, D.G., Young, L., Chuang, R.Y., Venter, J.C., Hutchison, C.A., 3rd, and Smith, H.O. (2009). Enzymatic assembly of DNA molecules up to several hundred kilobases. Nat. Methods *6*, 343–345.
41. Sturgill, E.G., Das, D.K., Takizawa, Y., Shin, Y., Collier, S.E., Ohi, M.D., Hwang, W., Lang, M.J., and Ohi, R. (2014). Kinesin-12 Kif15 targets kinetochore fibers through an intrinsic two-step mechanism. Curr. Biol. *24*, 2307–2313.
42. Hesse, W.R., Steiner, M., Wohlever, M.L., Kamm, R.D., Hwang, W., and Lang, M.J. (2013). Modular aspects of kinesin force generation machinery. Biophys. J. *104*, 1969–1978.
43. Shin, Y., Davis, J.H., Brau, R.R., Martin, A., Kenniston, J.A., Baker, T.A., Sauer, R.T., and Lang, M.J. (2009). Single-molecule denaturation and degradation of proteins by the AAA+ ClpXP protease. Proc. Natl. Acad. Sci. USA *106*, 19340–19345.
44. Khalil, A.S., Appleyard, D.C., Labno, A.K., Georges, A., Karplus, M., Belcher, A.M., Hwang, W., and Lang, M.J. (2008). Kinesin's cover-neck bundle folds forward to generate force. Proc. Natl. Acad. Sci. USA *105*, 19247–19252.
45. Gelles, J., Schnapp, B.J., and Sheetz, M.P. (1988). Tracking kinesin-driven movements with nanometre-scale precision. Nature *331*, 450–453.
46. Tarantino, N., Tinevez, J.Y., Crowell, E.F., Boisson, B., Henriques, R., Mhlanga, M., Agou, F., Israël, A., and Laplantine, E. (2014). TNF and IL-1 exhibit distinct ubiquitin requirements for inducing NEMO-IKK supramolecular structures. J. Cell Biol. *204*, 231–245.
47. Brady, S.K., Sreelatha, S., Feng, Y., Chundawat, S.P.S., and Lang, M.J. (2015). Cellobiohydrolase 1 from Trichoderma reesei degrades cellulose in single cellobiose steps. Nat. Commun. *6*, 10149.

## STAR★METHODS

### KEY RESOURCES TABLE

| REAGENT or RESOURCE | SOURCE | IDENTIFIER |
|---|---|---|
| Antibodies | | |
| His Tag Antibody, mAb | GenScript | Cat#A00186-100 |
| Penta-His Biotin Conjugate | QIAGEN | Cat#34440; RRID:AB_2714179 |
| Bacterial and Virus Strains | | |
| Bac-to-Bac Baculovirus Expression System | Thermo Scientific | Cat#10359-016 |
| BL21 DE3 | Novagen | Cat#69450 |
| *Spodoptera frugiperda* Sf9 cells | ThermoFisher Scientific | Cat#B82501 |
| Chemicals, Peptides, and Recombinant Proteins | | |
| FL-HSET | This paper; S.R.N. and R.O., unpublished data | N/A |
| HSET- ΔT | This paper; S.R.N. and R.O., unpublished data | N/A |
| HSET- ΔM | This paper; S.R.N. and R.O., unpublished data | N/A |
| Eg5 | [38] | N/A |
| Phusion DNA Polymerase | Thermo Scientific | Cat#F530L |
| Bovine Tubulin | Cytoskeleton | Cat#TL238 |
| PIPES | Sigma | Cat#P-1851 |
| EGTA | Sigma | Cat#E-4378 |
| $MgCl_2$ | Mallinckrodt | Cat#H590 |
| GTP | Cytoskeleton | Cat#BST06 |
| ATP | Sigma | Cat#A26209 |
| Bovine Tubulin | PurSolutions | Cat#1001 |
| Taxol | Cytoskeleton | Cat#TXD01 |
| Subtilisin | Sigma | Cat#P8038 |
| PMSF, phenylmethanesulfonyl fluoride | Sigma | Cat#P7626 |
| GMPCPP | Jena Bioscience | Cat#NU-405L |
| Rhodamine Tubulin | Cytoskeleton | Cat#TL590M |
| Biotinylated Tubulin | Cytoskeleton | Cat#T333P-A |
| Blotting Grade Blocker (casein) | BioRad | Cat#1706404 |
| Glucose Oxidase | Sigma | Cat#G2133 |
| β-D-Glucose | Sigma | Cat#G8270 |
| Catalase | Sigma | Cat#C40 |
| Streptavidin beads | Spherotech | Cat#SVP-05-10 |
| Sulfo-NHS | ThermoScientific | Cat#24510 |
| EDC | ThermoScientific | Cat#22980 |
| Ethanolamine | Sigma | Cat#E9508 |
| Poly-l-lysine | Sigma | Cat#P8920 |
| Oligonucleotides | | |
| 5′-biotin-TATTGCGTTTCCTCGGTTTC-3′ | IDT | N/A |
| 5′-amine-TTGAAATACCGACCGTGTGA-3′ | IDT | N/A |
| pFASTBAC-HTa-HSET Forward Primer: "pFB-HSET_UnlFOR": 5′-GTATTTTCAGGGCGCC ATGGATCCGGAATTCATGGATCCGCAGAGGTC-3′ | IDT | N/A |
| pFASTBAC-HTa-HSET Reverse Primer: "pFB-HSET_UnlREV": 5′-TCCTCTAGTACTTCTCGA CAAGCTTGGTACCTCACTTCCTGTTGGCCTG-3′ | IDT | N/A |

(*Continued on next page*)

*Continued*

| REAGENT or RESOURCE | SOURCE | IDENTIFIER |
|---|---|---|
| pFASTBAC-HTa-EGFP-HSETΔTail Forward Primer 1: "pFB-EGFP-FOR": 5′-GTATTTTCAGGGCGCCATGGA TCCGGAATTCATGGTGAGCAAGGGCGAGG-3′ | IDT | N/A |
| pFASTBAC-HTa-EGFP-HSETΔTail Forward Primer 2: "H139-GGS2-H673-FOR" 5′-CATGGACGAGCTGTACAAG GGAGGATCAGGAGGATCATTAAAGGGTCAGTTATGTGAC-3′ | IDT | N/A |
| pFASTBAC-HTa-EGFP-HSETΔTail Reverse Primer 1: "H139-GGS2-EGFPREV": 5′-GTCACATAACTGACCCT TTAATGATCCTCCTGATCCTCCCTTGTACAGCTCGTCCATG-3′ | IDT | N/A |
| pFASTBAC-HTa-EGFP-HSETΔTail Reverse Primer 2: "pFB-HSET_UnlREV": 5′-TCCTCTAGTACTTCTCGACAAGC TTGGTACCTCACTTCCTGTTGGCCTG-3′ | IDT | N/A |
| pET15b-HTa-EGFP-HSETΔMotor Forward Primer: "15b-_Cherry_IA_5": 5′-GCAGCGGCCTGGTGCCG CGCGGCAGCCATATGGTGAGCAAGGGCGAGG-3′ | IDT | N/A |
| pET15b-HTa-EGFP-HSETΔMotor Reverse Primer: "HSET304REV": 5′-CGGGCTTTGTTAGCAGCCGG ATCCTCGAGTCACAGCTGGTTGTGCAGTCG-3′ | IDT | N/A |
| Recombinant DNA | | |
| pET-15 | Novagen | Cat#69661 |
| M13mp18 | [39] | N/A |
| pFASTBAC1 | Thermo Scientific | Cat#10712-024 |
| pCR-Blunt II-TOPO-KifC1/HSET | Dharmacon | Cat# MHS6278-211690790 |
| pFASTBAC-HTa-HSET | This paper; S.R.N. and R.O., unpublished data | N/A |
| pET15b-HTa-EGFP-HSETΔMotor | This paper; S.R.N. and R.O., unpublished data | N/A |
| pFASTBAC-HTa-EGFP-HSETΔTail | This paper; S.R.N. and R.O., unpublished data | N/A |
| Software and Algorithms | | |
| MATLAB | MathWorks | https://www.mathworks.com |
| Msdanalyzer | MathWorks | https://tinevez.github.io/msdanalyzer/ |
| Other | | |
| Micro Bio-Spin 30 Column | BioRad | Cat#7326250 |

## CONTACT FOR REAGENT AND RESOURCE SHARING

Further information and requests for resources and reagents should be directed to and will be fulfilled by the Lead Contact, Matthew Lang (matt.lang@vanderbilt.edu).

## EXPERIMENTAL MODEL AND SUBJECT DETAILS

No cell or animal experiments were conducted.

## METHOD DETAILS

### Molecular Biology and Baculovirus Construction

HSET and HSET-ΔT were prepared using an HSET cDNA corresponding to Gen Bank Accession Number BC121041. HSET and HSET-ΔT plasmids were prepared in the baculovirus vector pFASTBAC-HTa (Life Technologies) for use with the insect cell expression system. HSET-ΔM was cloned into the bacterial expression vector pET15B (Novagen). Amino acid sequences of the tail, stalk, and motor domains of HSET/KIFC1 (*H. sapiens* kinesin-14) were determined by sequence alignment to Ncd (*D. melanogaster* kinesin-14) using [8] as a guide, and used to design pFASTBAC-HTa-EGFP-HSETΔT. pFASTBAC-HTa-EGFP-HSETΔT also contains a flexible amino acid linker (GGSGGS) to ensure rotational freedom between domains. Eg5 was prepared as described previously [38], and activity was confirmed by a gliding filament assay with an average velocity of 0.5 μm/min at 50 nM.

Each construct contains the corresponding amino acid sequence, which was verified by DNA sequencing:

pFASTBAC-HTa-EGFP-HSET: MSYY-$His_6$-YDIPTTENLYFQGAMDPEF-EGFP(aa 1-239)-HSET(aa 1-673).
pFASTBAC-HTa-EGFP-HSETΔT: MSYY-$His_6$-YDIPTTENLYFQGAMDPEF-EGFP(aa 1-239)-GGSGGS-HSET(aa 139-673).
pFASTBAC-HTa-HSET: MSYY-$His_6$-DYDIPTTENLYFQGAMDPEF-HSET(aa 1-673).
pET15B-HTa-EGFP-HSETΔM: MGSS-$His_6$-SSGLVPRGSH-EGFP(aa 1-239)-SGLRSRAQASNS-HSET(aa 1-304).

All constructs were prepared by isothermal assembly [40]. PCR fragments consisting of HSET amino acids 1-673 (pFASTBAC-HTa-EGFP-HSET, pFASTBAC-HTa-HSET), 139-673 (pFASTBAC-HTa-EGFP-HSETΔT), or 1-304 (pET15B-HTa-EGFP-HSETΔM) were generated by amplification of the HSET ORF (using pEGFP-C1-HSET as a DNA template [41] using Phusion DNA polymerase (New England Biolabs #M0530S). These fragments were then assembled into their expression vectors cut using the indicated restriction enzymes: pFASTBAC-HTa-EGFP-HSET: EcoRI/*XhoI*. pFASTBAC-HTa-EGFP-HSETΔT, pFASTBAC-HTa-HSET: EcoRI/*KpnI*. pET15B-HTa-EGFP-HSETΔM: *NdeI*/*XhoI* Constructs were used with the Bac-to-Bac system (Invitrogen) per manufacturers' protocol to create a baculovirus expressing the indicated protein.

## Protein Expression and Purification

Constructs in the pFASTBAC-HTa vector were expressed in *Sf9* cells by infecting them with the corresponding baculovirus for 72 hr. Constructs in the pET15B vector were expressed in BL21DE3 cells with 0.4 mM IPTG for 16 hr at 16°C. Each protein was purified via $His_6$-affinity chromatography, followed by size exclusion chromatography, as follows: cells were pelleted and resuspended in PNI buffer (50 mM sodium phosphate, 500 mM NaCl, 20 mM imidazole) with 5 mM β-mercaptoethanol (β-ME), 1% NP40, and protease inhibitors (1 mM phenylmethylsulfonyl fluoride, 1 mM benzamidine, and 10 μg/mL each of leupeptin, pepstatin, and chymostatin). Cells were then lysed by sonication and clarified by centrifugation at 4°C at 35K rpm for 1 hr in a Ti-45 rotor (Beckman). 4 mL of $Ni^{2+}$-NTA agarose (QIAGEN) were incubated with the supernatant for 1-2 hr, then washed extensively with wash buffer (PNI, 5 mM β-ME, 50 μM MgATP) for 3-4 hr. The proteins were then eluted from the $Ni^{2+}$-NTA agarose column in PNI with 5 mM β-ME, 180 mM imidazole, and 100 μM MgATP. Peak fractions (5 mL total) were then subjected to size exclusion chromatography on a Hiload 16/60 Superdex 200 preparatory grade column (GE Healthcare) in gel filtration buffer (10 mM K-HEPES, pH 7.7, 1 mM DTT, 300 mM KCl, and 100 μM MgATP). Protein concentrations were determined in mg/mL using Bradford assays (BioRad) and converted to molar units assuming dimer formation. Powdered sucrose was added to 20% w/v, then each protein was aliquoted, snap frozen in liquid nitrogen, and stored at −80°C.

## Microtubule Preparation

Tubulin was reconstituted and polymerized into microtubules as described previously [19]. Tubulin (bovine, Cytoskeleton TL238) was reconstituted in 25 μL PEM80 buffer (80 mM PIPES (Sigma P-1851), 1 mM EGTA (Sigma E-4378), 4 mM $MgCl_2$ (Mallinckrodt H590), pH adjusted to 6.9 with KOH) supplemented with 1 mM GTP (Cytoskeleton BST06) and kept on ice. Tubulin from PurSolutions (bovine, 1001) was also used and reconstituted in the supplied polymerization buffer. 13 μL PEM104 buffer (104 mM PIPES, 1.3 mM EGTA, 6.3 mM $MgCl_2$, pH adjusted to 6.9 with KOH), 2.2 μL 10 mM GTP, and 2.2 μL DMSO were mixed. 4.8 μL of 10 mg/mL tubulin were added to the mixture and allowed to incubate for 40 min at 37°C. Subsequently, 2 μL of stabilization solution (STAB, 38.6 μL PEM80, 0.5 μL 100 mM GTP, 4.7 μL 65 g/L $NaN_3$ (Sigma S-8032), 1.2 μL 10 mM Taxol (Cytoskeleton TXD01), 5 μL DMSO (Cytoskeleton)) was added to the stock microtubule solution at room temperature.

Microtubules with their E-hooks digested by subtilisin were also prepared as described previously [19]. Digested microtubules were made by removing the C-terminal E-hook of microtubules with subtilisin. 7.5 μL of pre-formed microtubules were mixed with 0.75 μL of 20 μM subtilisin (Sigma P8038) and was allowed to incubate at 37°C for 40 min. To stop digestion, 0.8 μL of 20 mM PMSF (phenylmethanesulfonyl fluoride, Sigma P7626) in DMSO was added to the digested microtubule mixture. 2 μL of STAB solution was then added to the digested microtubules at room temperature.

Polarity-marked microtubules were prepared by making a brightly fluorescent microtubule seed and polymerizing dimmer tubulin from that nucleation point. The microtubule seed was formed using GMPCPP, a non-hydrolysable analog of GTP (Jena Bioscience NU-405L). Rhodamine-labeled tubulin (Cytoskeleton, TL590M) was used in different concentrations to denote the bright seed from the dimmer elongation. First, the seed was polymerized by mixing 13 μL PEM104, 2.2 μL 10 mM GMPCPP, 2.2 μL DMSO, 4 μL non-labeled tubulin (10 mg/mL), and 1 μL rhodamine-labeled tubulin (10 mg/mL). The seed mixture was incubated at 37°C and allowed to incubate for 40 min. The elongation solution was made by mixing 13 μL PEM104, 2.2 μL 10 mM GTP, 2.2 μL DMSO, 2 μL non-labeled tubulin (10 mg/mL), and 1.5 μL rhodamine-labeled tubulin (1 mg/mL). The elongation mixture was incubated at 37°C for 1 min to ensure that the mixture was at least at room temperature. After the minute was complete, 1.5 μL of the seed mixture was added to the elongation mixture and allowed to incubate at 37°C for 40 min. Subsequently, 2 μL of STAB solution was added to the polarity-marked microtubules at room temperature.

## Single Molecule Optical Trapping Assays

0.44 μm streptavidin-coated beads (Spherotech, Lake Forest, IL) were prepared by washing with phosphate-buffered saline (PBS) followed by sonication. These beads were then incubated in 0.2 mg/mL biotinylated anti-His tag antibody (QIAGEN, Hilden,

Germany) to create anti-His coated beads. The beads were then washed 4 times with PBS by centrifuging at 10,000 rpm for 6 min to remove any unbound antibody. After gentle sonication, FL-HSET or HSET-ΔT constructs diluted in assay buffer (AB, PEM80 (80 mM PIPES (Sigma Aldrich, St. Louis, MO), 1 mM EGTA (Sigma Aldrich, St. Louis, MO), 4 mM $MgCl_2$ (Mallinckrodt, Dublin, Ireland), pH adjusted to 6.9 with KOH), 1 mM DTT (Sigma Aldrich, St. Louis, MO), 20 μM Taxol (Cytoskeleton, Denver, CO), 1 mg/mL casein (Blotting-Grade Blocker, Biorad, Hercules, CA), 1 mM ATP (Sigma Aldrich, St. Louis, MO))) were incubated with the biotinylated anti-His beads to allow binding of the N-terminal His-tag for 1 hr at 4°C on a rotator in the presence of oxygen scavenging reagents (5 mg/mL β-D-glucose (Sigma Aldrich, St. Louis, MO), 0.25 mg/mL glucose oxidase (Sigma Aldrich, St. Louis MO), and 0.03 mg/mL catalase (Sigma Aldrich, St. Louis, MO)).

Flow cells with an approximate volume of 15 μL were constructed by attaching an etched coverslip to a microscope slide with two strips of double-sided tape. Before flow cell construction, the etched slide was incubated with poly-l-lysine (Sigma Aldrich, St. Louis, MO) for subsequent microtubule attachment. After assembly, microtubules were diluted 100-200 times in PemTax (0.02 mM Taxol in PEM80), added to the flow cell, and incubated for 10 min. The flow cell was then washed with 2 volumes of PemTax to remove any unbound microtubules. Casein diluted in PemTax to 1 mg/mL was then added and incubated for 10 min to reduce any non-specific binding. 5 volumes of PemTax were then added to wash out any unbound casein, followed by 8 volumes of AB. 2 volumes of the bead/motor solution described above were then added to the flow cell.

Optical trapping measurements were obtained using a custom built instrument described previously [42–44]. Bead displacements from the trap center were recorded at 3 kHz and anti-alias filtered at 1.5 kHz. Position and trap stiffness calibrations were measured using custom Labview (National Instruments) programs. The single molecule limit of the assay was determined through serial dilution of the motor constructs such that fewer than half of the beads trapped bound to microtubules, with an actual binding percentage of about 10% [21]. In loaded motility assays, beads were trapped in solution where position and trap stiffness calibrations were performed. Subsequently, the bead was brought to a microtubule adhered to the coverslip surface to allow for binding. Displacement and force generation were then measured for single motor-bound beads. In unloaded motility assays, beads are trapped in solution and brought to a microtubule. The trapping laser in turned off, and the motion of the bead is then video-tracked with a DAGE CCD camera. Cross-correlation methods were used to track bead positions over time through custom MATLAB code [39, 43, 45]. The step/dwell finding algorithm was used to determine preference for motility in either direction. Here, a step threshold of 200 nm was used to account for geometric wobble of the 440 nm bead through the tethering point. Sequential steps in the same direction were added together until the step changed directions, where the process was repeated until the end of the trace. Mean squared displacement (MSD) analysis of unloaded traces was performed using the MATLAB plug-in msdanalyzer [46]. MSDs were then averaged over 1 s intervals.

Tail binding measurements were obtained by pulling on beads tethered to microtubules through the tail domain. The tail domain was tethered to streptavidin beads by a 1,010 base pair DNA linker functionalized with biotin on one end and a terminal amine on the other. The 1,010 bp DNA linkers were created as described previously [19]. The amine was further crosslinked to anti-His antibody (GenScript, Piscataway, NJ) using sulfo-NHS/EDC chemistry (ThermoScientific), as described previously [19]. The diluted beads in a 100 μL volume were incubated with 1 μL of diluted 100x diluted DNA linker (25 ng/μL stock) and 1 μL 100x diluted tail-stalk (10 μM stock) for 1 hr. Flow cells were created as described above. In the final step, the tethered beads were added. Beads were then trapped in solution and brought close to microtubules to allow for tether formation. The piezostage was then moved in 200 nm steps at 2 μm/s to sufficiently elongate the DNA tether and impart force on the interaction, holding the interaction at a desired force. Single ruptures were characterized through a single, uninterrupted return to baseline after the force ramp.

Measurement of force generation in polarity-marked microtubule bundles was performed as described previously [19]. Briefly, fluorescent polarity-marked microtubules were added to a poly-l-lysine coverslip in a flow cell and allowed to incubate for 10 min. After washing with buffer, casein was used to block the remainder of the surface to prevent non-specific binding and incubated for 5 min. While the first two steps incubated, diluted 1.25 μm streptavidin coated beads were incubated with concentrated biotin seed microtubules (minus end biotinylated seed formed with GMPCPP, non-labeled tubulin polymerized from the seed to form an elongation) in the presence of oxygen scavenging reagents. The bead/microtubule solution was then diluted 100x, and the appropriate ratio of motor (Eg5:HSET) was added. The bead/microtubule/motor solution was then quickly added to the flow cell. Force and displacement measurements were recorded within 30 min of the final addition. Bundle orientation was determined by knowing the location of the trap center (streptavidin bead will only by the biotinylated minus end of the top microtubule) and the relative location of the fluorescent polarity marked microtubule on the bottom.

Calibration and trap stiffness data were used to determine the displacement and force generation with resolution at the nm and pN levels, respectively. Motility traces, and stall forces therein, were visualized using custom-written MATLAB code as described previously [42–44]. Other codes were used to determine lifetimes, velocities, run lengths, and force-velocity relationships. A step/dwell-finding algorithm based on a sliding Student's t test was used to determine the edge of each step so that a dwell was defined in between [47]. Decay constants were used to describe dwell times. A step threshold of 3 nm was imposed due to the defined step sizes of most kinesins being around 8 nm but also allowing for variation without detecting noise. The force-velocity behavior of FL-HSET was calculated by averaging force over 5 s windows, and the average velocity for each window was calculated using a linear fit. The data were then fit to the one parameter Boltzmann model [22].

## QUANTIFICATION AND STATISTICAL ANALYSIS

All experiments were repeated until convergence and high N to ensure that the data were robust. Histograms are presented as probability distributions for that certain event to occur. Average and standard deviation are reported throughout the paper and figure legends. Error bars are standard error unless stated otherwise. The N value for each experiment is reported in each figure. N represents: number of stalls (Figure 1E), number of steps (Figure 1C, Figure 2D), number of dwells (Figure 1D, Figure 2E), number of run length measurements (Figure 2D), number of lifetime measurements (Figure 3B, Figure 3E), number of rupture events (Figure 3C, Figure 3F), number of parallel bundle measurements (Figure 4B), number of anti-parallel bundle measurements (Figure 4B), and number of mixed bundle traces (Figure 4C). In the custom written algorithms used for analysis, a sliding Student's t test was used to determine boundaries (steps, dwells, stalls, change in direction) in each trace. One-way ANOVA was performed on unloaded velocity and run length between HSET and HSET-deltaT (Figure S2), as well as plateau forces in different bundle ratios (Figure S3). p values are provided in figure captions and indications of non-significance (n.s.).